ADVANCED SUSTAINABLE SYSTEMS
www.advsustainsys.com

Nanofluid Based on Glucose-Derived Carbon Dots Functionalized with [Bmim]Cl for the Next Generation of Smart Windows

Helena M. R. Gonçalves, Rui F. P. Pereira, Emmanuel Lepleux, Thomas Carlier, Louis Pacheco, Sónia Pereira, Artur J. M. Valente, Elvira Fortunato, Abel J. Duarte, and Verónica de Zea Bermudez**

The design of new advanced materials and technologies is essential for the development of smart windows for the next generation of energy-efficient buildings. Here, it is demonstrated that the functionalization of glucose-derived carbon dots with 1-butyl-3-methylimidazolium chloride results in a self-standing, water-soluble, viscous, reusable nanofluid with self-improving conductivity, thermotropy around 30–40 °C, and ultraviolet blocking ability. Its synthesis is straightforward, clean, fast, and cheap. At 36 °C (hot summer day), a sun-actuated thermotropic (TT) device incorporating a 95% w/w nanofluid aqueous solution exhibits a transmittance variation (ΔT) of 9% at 550/1000 nm, which is amplified to 47/31% via the surface plasmon resonance effect. An integrated self-healing system enabling independent sun-actuated TT and voltage-actuated electrochromic (EC) operation is also produced. The low-energy EC device offers bright hot and dark cold modes (ΔT = 68/64%), excellent cycling stability, unprecedented coloration efficiency values ($-1.73 \times 10^6/-1.67 \times 10^6$ cm^2 C^{-1} (coloring) and $+1.12 \times 10^7/+1.08 \times 10^7$ cm^2 C^{-1} (bleaching) at ±2.5 V), and impressive memory effect. The disruptive design and sustainable synthesis of the new nanofluid proposed here will foster the agile development of novel products with improved ecological footprint.

1. Introduction

Energy and nanotechnology go hand in hand and both play a crucial role in society. In recent years, population growth, fast urbanization, and technological development resulted in a substantial increase of energy demand. The pressing need for a dramatic reduction of anthropogenic energy consumption and the transition to a greener energy scenario has prompted many countries to launch several initiatives.[1] The "Sustainable Development Goals" are the blueprint to ensure universal access to affordable, reliable, sustainable, and modern energy by 2030.[2]

The building sector is part of the energy solution. Buildings represent the world's largest energy consuming economic sector. In USA, buildings consume roughly 40% of all input energy used.[3] Windows, which are responsible for ≈10% of this energy,[4] will play a major role in curbing the building's energy loss. Estimates indicate that the replacement of classical windows by smart ones may result in a 40% reduction of the building's energy needs.[3] Not surprisingly, the development of smart switchable glazing has witnessed an upsurge of interest in recent years.[5] Current research aims at fabricating smart windows applicable across different types of buildings and climate zones, enabling the fine-tuning of sunlight transmittance (visible radiation) and solar heat gain (near-infrared (NIR) radiation). Both parameters have high impact on energy use, indoors thermal and visual comfort, and outdoors view.[3]

Dr. H. M. R. Gonçalves, Prof. V. de Zea Bermudez
Chemistry Department and CQ-VR
University of Trás-os-Montes e Alto Douro
5001-801 Vila Real, Portugal
E-mail: helenardrgs@gmail.com; vbermude@utad.pt
Dr. H. M. R. Gonçalves, Prof. A. J. Duarte
REQUIMTE
Instituto Superior de Engenharia do Porto
4200-072 Porto, Portugal
Dr. R. F. P. Pereira
Chemistry Department and Chemistry Centre
University of Minho
4710-057 Braga, Portugal
The ORCID identification number(s) for the author(s) of this article can be found under https://doi.org/10.1002/adsu.201900047.
E. Lepleux, Dr. T. Carlier, L. Pacheco
CSInstruments (CSI-AFM France)
91940 Les Ulis, France
Dr. S. Pereira, Prof. E. Fortunato
CENIMAT/I3N
Departamento de Ciência dos Materiais
Faculdade de Ciências e Tecnologia
Universidade NOVA de Lisboa
2829-516 Lisboa, Portugal
Prof. A. J. M. Valente
CQC
Chemistry Department
University of Coimbra
3004-535 Coimbra, Portugal

DOI: 10.1002/adsu.201900047

Chromogenic materials have been at the core of smart switchable architectural glazing. In these materials, an external stimulus triggers a change of the optical properties.[6] Several chromogenic technological solutions have been implemented at a small scale. Deploying dynamic windows in every building of the planet is, however, a challenging goal which will only be attained if high-tech materials are further developed, while ensuring sustainability assets. This effort calls for new designs and synthesis strategies, and for radical new concepts and paradigms of materials science.

Herein, we demonstrate an innovative nanotechnology-based platform offering tremendous opportunities for the field of smart windows. It relies on the use of a nanofluid composed of glucose-derived carbon dots (Cdots) functionalized with the 1-butyl-3-methylimidazolium chloride ([Bmim]Cl) ionic liquid (IL).

ILs are unique compounds with tremendous technological interest. They are particularly suitable for eco-friendly energy applications.[7–11] As they may act as solvents, reactants, or structure directing agents, ILs are advantageous for materials synthesis.[12] The widely used [Bmim]Cl was selected for several reasons: 1) its nontoxicity[13] makes it favorable for application in the building sector; 2) it exhibits a reversible thermotropic (TT) effect at 30 °C[14] associated with a *trans–trans* to *trans–gauche* conformational change of the butyl chain;[15] and 3) it has strong hydrogen bond–accepting ability imparted by the Cl^- ion.[16–18]

Cdots are carbon-based nanomaterials with outstanding attributes.[19] They show great prospects for energy applications, but research in this domain is still at infancy. Their optical features are particularly appealing. Tailoring Cdots size allows fine-tuning of their excitation/emission features.[20] Moreover, their absorption/transmission properties may be greatly enhanced via the surface plasmon resonance effect (SPRE). Furthermore, Cdots are generally composed of amorphous and graphitic carbons, and hence surface plasmons can be observed among sp^2 hybridized carbon atoms, which will significantly enhance the plasmonic effect.[21,22] Another advantage of Cdots is the possibility of producing them from carbohydrates which are abundant in nature, have low carbonization temperatures, and are nontoxic.[23] A critical drawback of carbon nanomaterials is that they usually require expensive and time-consuming pretreatments to make them hydrophilic.[24] Although their dispersibility in water has been greatly improved by surface modification and the use of surfactants, these are expensive and low-yield methods.[24]

The association of [Bmim]Cl with Cdots led to the formation of a non-Newtonian TT nanofluid, water-soluble, reusable, and exhibiting self-improving behavior. Typical nanofluids are described as stable suspensions of nanoparticles (NPs) in conventional base fluids.[25] Nanofluids present several advantages over the base fluid, such as superior heat transfer rates[26] which may become unusually high whenever the nanofluid exhibits a non-Newtonian behavior.[27]

We envisioned that this nanofluid would own great potential for the energy area, and, in particular, for the smart windows technology. There are broadly two types of smart windows: environmentally activated and electrically activated. An environmentally activated smart window (or passive window) does not require electric supply as its operation depends exclusively on natural sunlight. These sort of windows can be further classified as photochromic, thermochromic, and TT. In contrast, an electrically activated smart window (or active window) requires electric supply. Electrochromic (EC), liquid crystal, and suspended particle (SP) smart windows belong to the latter category. It is worth referring at this stage a breakthrough technology introduced recently using fluidic windows based on thermoactive building systems (TABS).[28] This concept has proved to be an effective alternative to help reducing the energy input of buildings. This technology relies on channels for the circulation of the fluid, which acts as both reservoir and transport system to harvest external heat and solar energy.[29] The channels can be incorporated into the building infrastructure (e.g., walls, ceilings, and floors), thereby transforming them into thermally active components.[30] The windows are basically low cost, switchable, ultrathin SP devices (SPDs) suitable for large-area integration with smart façades. The circulating fluid incorporates magnetic nanoparticles enabling active shading and solar-thermal energy harvesting. The loading state and the optical properties of the liquid are controlled through remote switching in a particle collector-suspender device. In comparison to the classical SPD concept, this solution does not require electrical contacts, transparent conductive layers, or electrolytes. However, despite the fact that these windows do provide efficient glazing control, the production of the microchannel structure where the fluid will circulate is compulsory, and energy must be provided for fluid circulation.

To test the potential of our nanofluid as a disruptive material for smart windows technology, we decided to evaluate its performance in two prototype devices: a sunlight-actuated TT device (TTD) with SPRE-enhanced performance, and an integrated TTD/EC device (ECD) system independently operated by sunlight/voltage. Our findings evidence the tremendous interest in the nanofluid for the fabrication of self-healing smart devices extremely easy to be fabricated, endowed with visible/NIR control ability, and featuring various impressive figures of merit.

2. Results and Discussion

2.1. Design, Synthesis, and Characterization of the Nanofluid

Here, we show that the Cdots synthesis from glucose and their functionalization with [Bmim]Cl, by means of a one-pot hydrothermal method using a simple, straightforward, single-step procedure, under mild reaction conditions, are possible. [Bmim]Cl acted both as reaction medium and functionalization molecule (**Figure 1**). Hydrothermal methods for Cdots production usually require, regardless of the raw material, temperatures above 200 °C, reaction times slower than 3 h, and high pressures.[31,32] The introduction of [Bmim]Cl allowed for an easily scalable and faster synthesis (1 h), lowering the temperature to 100 °C at atmospheric pressure, ruling out expensive and complex equipment.

The preparation of Cdots by hydrothermal carbonization of carbohydrates generally occurs through rupture of the N-linkages until low molecular weight organic molecules are formed.[33] During this process, small nucleation clusters are

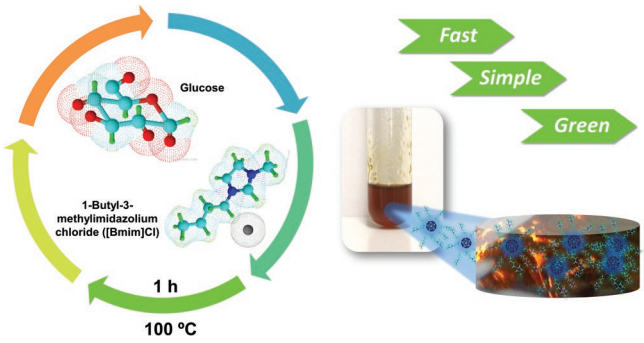

Figure 1. Synthesis of the nanofluid. Schematic representation of the nanofluid synthesis, using anhydrous glucose as starting material and 1-butyl-3-methylimidazolium chloride as both reaction medium and functionalization molecule.

formed leading to the NPs formation. The NP size increases with reaction time until a stable value is reached that allows them to remain suspended in the reaction media. [Bmim]Cl plays a twofold role. Because of its low interfacial tension, the nucleation rate increases, facilitating the formation of smaller particles. Additionally, its low interface energy helps stabilizing the produced Cdots, preventing their aggregation.[34] The water content in the IL interferes significantly with the size of NPs, as it must be kept below 10% to guarantee functionalization.[35] For this reason the amount of water was thoroughly controlled and a brown viscous nanofluid resulted (Figure 1). Elemental analysis demonstrates that the nanofluid contains, as expected, 44% of carbon and 11% of nitrogen (Figure S1, Supporting Information). Scanning electron microscopy (SEM) images (**Figure 2**a,b) are consistent with the different chemical composition of the spherical Cdots and the [Bmim]Cl surrounding them (Figure S2a,b, Supporting Information). To observe the individual NPs, high-resolution transmission electron microscopy (HR-TEM) was performed. The images show homogeneous, well-defined, and spherical Cdots (Figure 2c). Their mean size, determined by dynamic light scattering (DLS), is 6.8 nm (Figure S3, Supporting Information), which is the typical value for NPs synthesized in the presence of an IL with low water content. The functionalized Cdots exhibit a lattice spacing of 0.24 nm (inset of Figure 2c) associated with the (020) plane of graphite.[36] Atomic force microscopy (AFM) (Figure 2d–f) reveals 535 particles in a $10 \times 10\ \mu m^2$ area and a quite low roughness of 1.877 nm.

Based on the DLS data and on the masses of carbohydrate and IL employed, we estimated that the Cdots have around 37 [Bmim]Cl molecules at their surface and that the surface

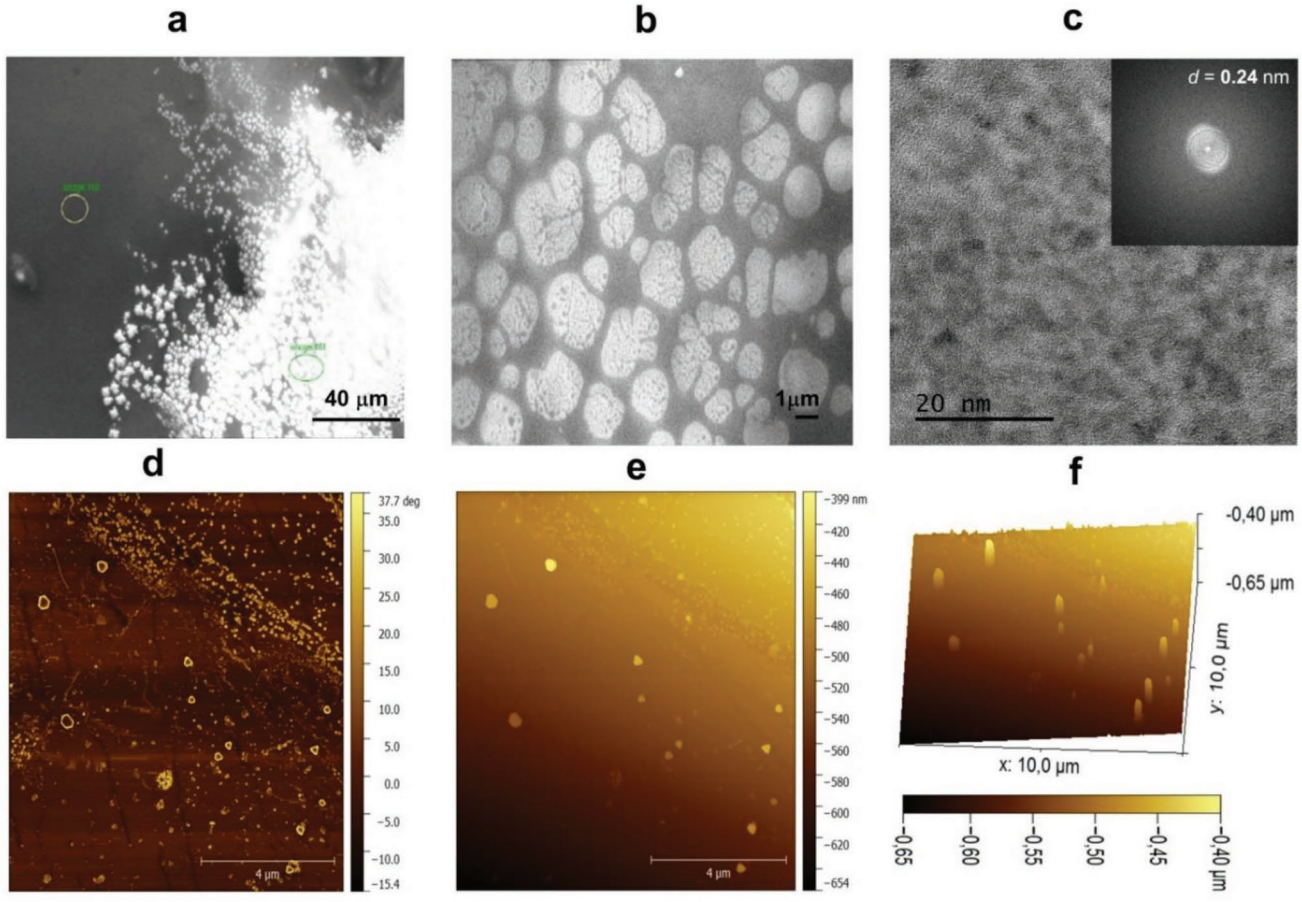

Figure 2. Structure and morphology of the nanofluid at the nanoscale. a,b) SEM and c) HR-TEM images. Fast-Fourier transformation of the TEM image (inset of (c)) allowed the determination of a 0.24 nm characteristic distance. d) AFM phase, e) 2D topographical, and f) 3D topographical images obtained in resonant mode. EDS analyses of the areas highlighted in (a) are given in Figure S2a,b in the Supporting Information.

charge density is ≈1.10 × 10^{15} cm^{-2}. These values are in perfect agreement with those of Sun et al.[37] However, a reaction temperature of 180 °C, pyrolysis, and a multistep procedure were required by these authors to obtain Cdots with similar surface characteristics. Further characterization revealed a weight loss of 8% below 300 °C in the nanofluid thermogravimetric analysis (TGA) curve (Figure S4, Supporting Information) which is associated with the decomposition of the oxygen-containing moieties of small molecules weakly bonded to the Cdots surface. The sharp weight loss at 320 °C is attributed to the decomposition of the [Bmim]Cl molecules located at the Cdots surface. These results confirm the functionalization of the Cdots surface with different chemical species (very likely hydroxyl (−OH), $[Bmim]^+$ and Cl^-), and reveal that [Bmim]Cl exerts a stabilizing effect on the Cdots. The Cdots Zeta Potential is negative and low, indicating the occurrence of small NPs stable in solution (Figure S5, Supporting Information). Moreover, it increased with temperature, proving that the stability of the Cdots in the nanofluid increases with temperature.

The conductivity of the nanofluid ranges from 0.46 to 2.8 mS cm^{-1} at 24 and 58 °C, respectively (**Figure 3**a). In general, ILs exhibit lower conductivities than their corresponding concentrated aqueous electrolyte solutions, due to the decrease of ion mobility and of the proportion of available charge carriers.[38] The combination of ILs with Cdots is an innovative and efficient way of overcoming this drawback, since the nanofluid exhibits higher conductivity than the 95% w/w nanofluid aqueous solution (inset of Figure 3a). The exact nature of the charge carriers is unknown at present. However, considering that Cl^- ions are prone to hydrogen bond to −OH groups at the surface of the Cdots in the case of the nanofluid, and also to water molecules in the case of the aqueous solution, it is highly likely that the conductivity measured is correlated with the transport of protons via Grotthuss hopping and/or vehicular mechanism. We cannot discard, however, the fact that Cdots have naturally occurring surface defects, traps, and holes which provide interesting substrates for nanoscale conductivity.

We note that the conductivity of the nanofluid and of the 95% w/w nanofluid aqueous solution demonstrated nonreversible hysteresis behavior upon consecutive heating/cooling cycles, the effect being more marked in the latter material. The initial conductivity value was never recovered and became higher with cycling, denoting an appealing self-improving feature (Figure 3b).

The dynamic viscosity of the nanofluid, measured under stirring (100 rpm), decreased progressively with the increase of temperature in a reproducible way (Figure 3b). On cooling the nanofluid to 25 °C after heating it to 60 °C, the dynamic viscosity showed hysteresis, but the system did not attain its initial value, demonstrating a non-Newtonian behavior. A drastic viscosity decrease of 80% and 93% occurred after the 1st and 2nd cycles, respectively (Figure 3b). Yet, no changes were detected overtime in the absence of heating, a proof of the stability of the nanofluid. In the case of non-Newtonian nanofluids based on carbon nanotubes, the increase of the effective dynamic viscosity with time was ascribed to NP aggregation induced by the surface electron charge and strong van der Waals forces.[39] In this work, the viscosity did not change unless heat was provided and the formation of aggregates was not visible. Therefore, these results provide strong evidence that the viscosity temperature dependence of the present nanofluid is solely due to the Cdots characteristics rather than to an aggregation phenomenon.

We associate the nanoscopic conductivity and viscosity memory effects described above, and the nonreversibility of the hysteresis with the disruption/reformation of the hydrogen-bonded array[40] existent in the nanofluid and in its aqueous solution. Indeed, the Cdots surface groups tend to hydrogen bond to the Cl^- ions in the nanofluid, and also to water molecules in the 95% w/w aqueous solution. When the sample is heated above the [Bmim]Cl TT transition temperature (T_t), two processes operate concomitantly: the extended-to-coiled butyl chain conformational change, and the annihilation of the hydrogen-bonded network. During cooling, the reformation of the same hydrogen bonds is unlikely. Moreover, the chain conformational transformation, which is a reversible phenomenon in the case of pristine [Bmim]Cl, is constrained in the nanofluid.

This explanation agrees with the fact that the hysteresis is much more marked in the case of the 95% w/w nanofluid aqueous solution (inset of Figure 3a) than in the nanofluid itself (Figure 3a).

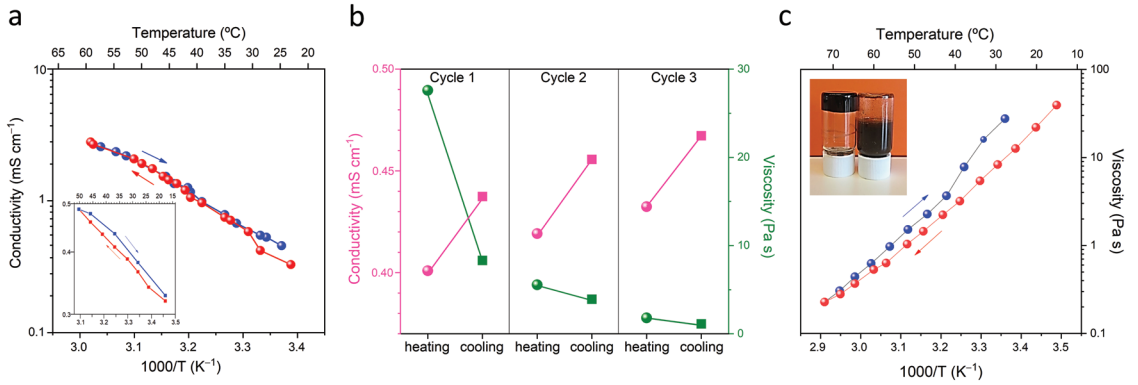

Figure 3. Conductivity and dynamic viscosity of the nanofluid. a) Arrhenius conductivity of the nanofluid in the 1st heating (red symbols)/cooling (blue symbols) cycle. Inset of (a): Arrhenius conductivity of the 95% w/w nanofluid aqueous solution. b) Conductivity (left *y*-axis pink symbols) and dynamic viscosity (right *y*-axis, green symbols) of the nanofluid measured at 25 °C over the first three heating (circles)/cooling (squares) cycles. c) Arrhenius dynamic viscosity of the nanofluid in the 1st heating (red symbols)/cooling (blue symbols) cycle. Inset of (c): Photograph of the nanofluid below (left) and above (right) the thermotropic transition temperature. The lines drawn are guides for the eyes.

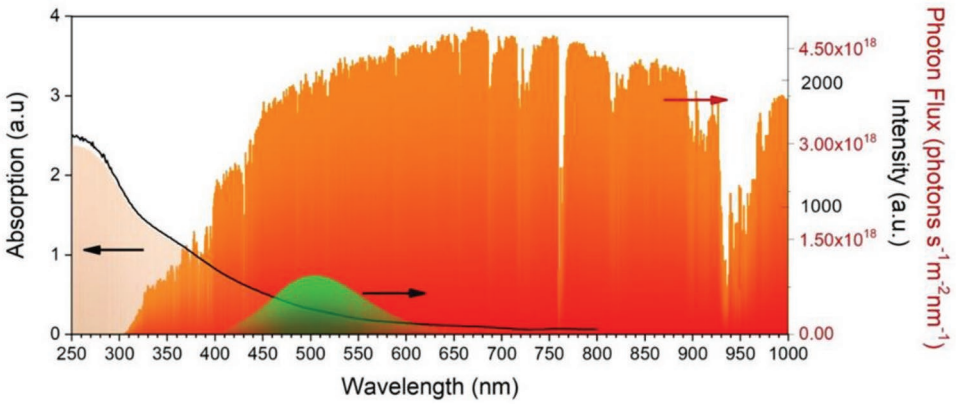

Figure 4. Optical features of the nanofluid. Absorption spectra at 25 °C (left axis, light brown area) and 50 °C (left axis, black line); Fluorescence emission spectrum excited at 400 nm (right axis, green area); AM1.5G photon flux (right axis, red–orange area) recorded with a solar simulator (model 10500, Abet Technologies).

The nonrecovery of the initial values of conductivity and viscosity reveal that the nanofluid is a complex system[41,42] characterized by self-organization.[43] Heat perturbs the nanofluid acting like a "quake,"[44] pushing it to a metastable state, different and less stable than the initial state, and inducing irreversible changes in all its properties. After heat removal, the stressed nanofluid tries to relax, and its components seek collective coherent arrangements to reach a more stable state. Each new heating cycle sends the nanofluid to a completely different metastable state.

Neither the Cdots optical absorption nor the fluorescence emission are due to an intrinsic band gap. Indeed, because of their sp^2 hybridized carbon atoms plasmons, and radiative recombination of the surface-confined electrons and holes, the changes in the Cdots absorption and fluorescence properties originate from a process different from that of semiconductor quantum dots.[45,46] Nonetheless the Cdots possess a broad excitation/emission band, and a weak ultraviolet UV–vis absorption tail extending from the maximum peak absorption at 263 nm (**Figure 4**) to the visible region of the solar spectrum (Figure 4). This feature is particularly important in smart window applications, because the TT nanofluid can act as UV harvest unit, blocking UV from reaching indoors. Interestingly, this UV–vis absorption is temperature-dependent (Figure 4), pointing out the potential of this nanofluid as UV harvest unit during daytime temperature fluctuations.

2.2. TT Devices

TT materials change their light scattering properties with temperature, switching from a transparent off-state to a light scattering on-state when the temperature of the window glass is below or above the T_t of the material, respectively.[47] TTDs are passively switching systems with high solar modulation, sunlight-driven, self-regulating and thus virtually zero-energy consumption (**Figure 5**a). TTDs involve maintenance-free

Figure 5. Schematic representation of the operation of a window glass incorporating the SPRE-enhanced TTD a) or the integrated TTD/ECD system b) proposed here. Outside view at 25 °C I), 36 °C II), 50 °C III), 60 °C IV), and –2.5 V V).

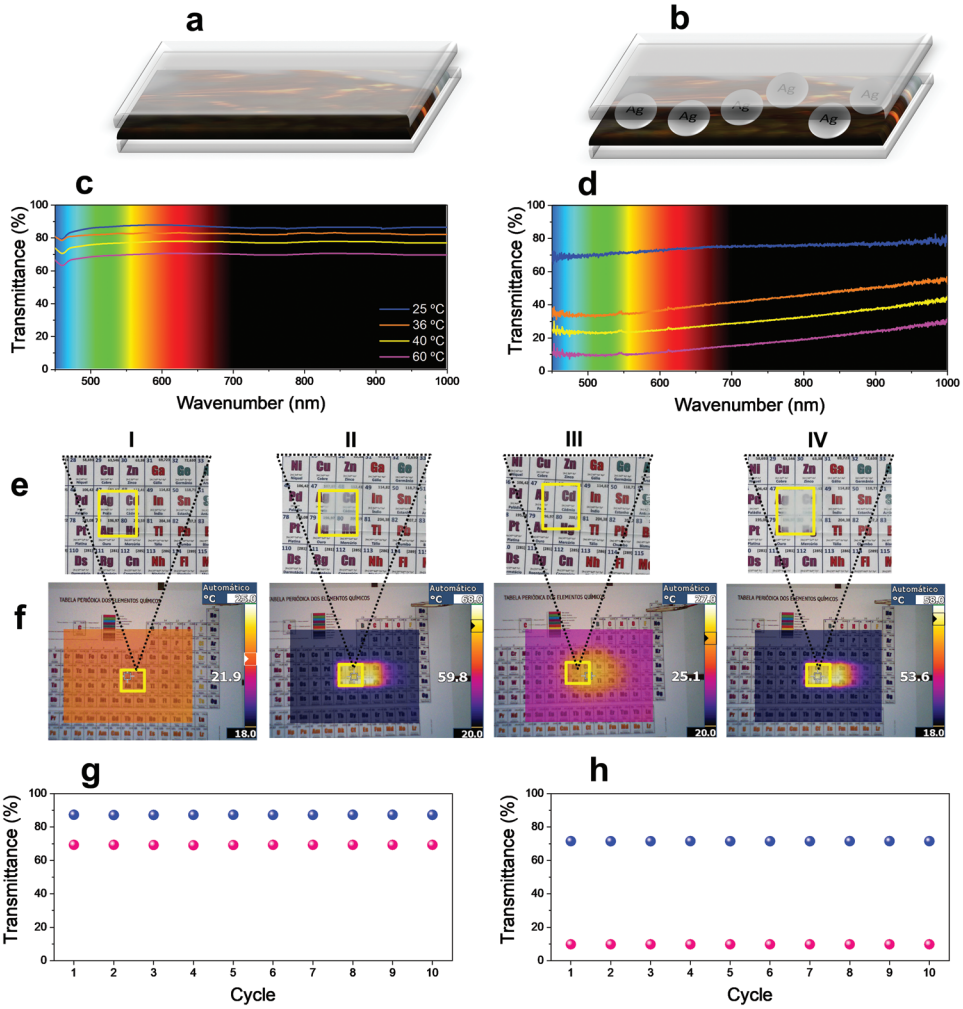

Figure 6. Performance of the glass/95% w/w nanofluid aqueous solution/glass (left) and SPRE-enhanced glass/95% w/w nanofluid aqueous solution/Ag/glass (right) TTDs. Schematic representation of the devices a,b) and temperature dependence of the transmission spectra c,d). Visible e) and infrared f) photographs of both devices at room temperature I,III) and above the TT transition temperature II,IV). Cycling stability at 550 nm g,h).

low-cost products, with variable shape and size, high long-term stability, and easy installation.[48] T_t should be close to room temperature for the window to be energy efficient. TTDs are applicable in areas where obstructed view is irrelevant, such as skylights, roof lights, upper windows, inclined glazing, privacy glazing, and façade elements.

To test the performance of a TTD incorporating the nanofluid, a 95% w/w nanofluid aqueous solution was simply sandwiched between two plain glass plates (**Figure 6**a). The TTD transmittance (T in %) decreased with temperature (Figure 6c,e,f (I,II)), corroborating the absorption data. The T value reduction at 36 °C confirms that the [Bmim]Cl TT transition is retained in the nanofluid. The switching efficiency ($\Delta T_{TT} = T_{T<T_t} - T_{T>T_t}$) at 36, 40, and 60 °C were 4, 9%, and 17%, respectively, at 550 and 1000 nm (**Table 1**).

The TT behavior was extraordinarily enhanced via SPRE. The plasmonic interaction of metal NPs with light can boost the performance of solar radiation absorption.[47,48] When these NPs are in contact with highly conducting Cdots, the effect is outstanding. A second TTD was assembled in which one of the glass plates was decorated with silver (Ag) islands[45,49] (Figure 6b). The excitation of the nanofluid plasmons and their transformation into propagating photons boosted the TT phenomenon (Figure 6d–f (III,IV)) with respect to the Ag-free TTD. At exactly the above temperatures, impressive ΔT_{TT} values of 37/21, 47/31 and 61/55% resulted at 550/1000 nm (Table 1).

Figure 6g,h demonstrates the good stability of both TTDs over 10 heating/cooling cycles.

2.3. Integrated TT/EC Device

EC materials change their optical properties in a reversible and persistent way upon application of a small voltage (usually 1–3 V). The window remains transparent at all times during the modulation of transmitted daylight and solar heat gains. The archetypal EC device multilayer sandwich configuration is composed of external transparent conducting oxides (TCOs), an EC film, an ion conductor (IC), and an ion storage (IS) layer. In general, ECDs offer a transparent (bleached) off-state, and

Table 1. Optical parameters of the TTDs in the plain and plasmonic modes, and electro-optical parameters of the ECD mode of the integrated TTD/ECD system. $T/\Delta T$ and CE values are given in % and $cm^2\ C^{-1}$, respectively.

λ [nm]	TTD_{plain}							$TTD_{plasmonic}$						
	$T_{25\ °C}$	$T_{36\ °C}$	ΔT_{TT}	$T_{40\ °C}$	ΔT_{TT}	$T_{60\ °C}$	ΔT_{TT}	$T_{25\ °C}$	$T_{36\ °C}$	ΔT_{TT}	T40 °C	ΔT_{TT}	$T_{60\ °C}$	ΔT_{TT}
550	87	83	4	78	9	70	17	71	34	37	24	47	10	61
1000	86	82		77		69		76	55	21	45	31	21	55

ECD					
$T_{bleached}$	$T_{colored}$[a)]	ΔT_{EC}	ΔOD	CE_{in}[b)]	CE_{out}[b)]
72	4	68	1.2	-1.73×10^6	$+1.12 \times 10^7$
70	6	64	1.1	-1.67×10^6	$+1.08 \times 10^7$

[a)]After 210 CA cycles; [b)]Measured on the 210th cycle.

one (or several) colored on-state(s), as a result of reduction/ion insertion and oxidation/ion disinsertion processes taking place in the EC and IS, respectively. As EC windows require extra electric energy to drive the transparency/color switch, they may be addressed as low-energy consumption devices.[50] EC windows offer modulation of sunlight over a broad spectral range, controllable transmission, absorption and/or reflectance, and open-circuit memory (Figure 5b). During operation, outside view is never obstructed.

In the present work we envisaged the production of an integrated TTD/ECD system featuring independent operation. It would be either sun-actuated (TT mode) or manually-actuated (ECD mode) whenever decided by the user. The new device concept introduced here implies the use of an amorphous tungsten oxide (a-WO_3) EC film, a crystalline nickel oxide (c-NiO) IS layer, the 95% w/w nanofluid aqueous solution as IC, and external TCOs of amorphous indium zinc oxide (a-IZO) (**Figure 7**a). The latter oxide is transparent in the visible and NIR[51] and exerts tremendous benefits on the performance of ECDs.[52,53]

The integrated device was subject to cyclic voltammetry (Figure S6, Supporting Information) and chronoamperometry (CA) cycling (±2.5 V, 50 s intervals) (Figure 7c) to evaluate its performance at room temperature. Switching efficiency ($\Delta T_{EC} = T_{bleached} - T_{colored}$) values of 68/64% and optical density ($\Delta OD = -\log (T_{colored}/T_{bleached})$) values of 1.2/1.1 resulted at 550/1000 nm (Figure 7b and Table 1). The anodic and cathodic current densities have practically the same value that remained constant, demonstrating excellent stability (inset of Figure 7c). During coloration, the cathodic current returned to zero. In contrast, during bleaching, the anodic current never returned to zero. We associate this residual current with the resistance offered by the c-NiO/a-IZO plate to the passage of the electric field due to the NiO crystallinity and surface roughness.[51] CA measurements were pursued after separating apart both plates and joining them back together (video). The performance of the reconstructed device was not affected, confirming the good mechanical and adhesion properties of the 95% w/w nanofluid aqueous solution. Moreover, upon application of −2.5 V, the ECD remained in the colored state over a month under open circuit with minimal coloration loss, denoting an exceptionally good performance (Figure 7d). The CE ($CE = \Delta OD/\Delta Q$, Q being the inserted/disinserted charge density) values are colossal: $-1.73 \times 10^6/-1.67 \times 10^6\ cm^2\ C^{-1}$ for coloration and $+1.12 \times 10^7/+1.08 \times 10^7\ cm^2\ C^{-1}$ for bleaching at 550/1000 nm. Figure 7e confirms that the TTD and ECD modes operate independently. Indeed, coloring was temperature-independent and scattering was voltage-independent. This means that under ECD operation Joule heating did not induce a scattering change.

3. Conclusions

Here, we show that a non-Newtonian nanofluid based on [Bmim]Cl-functionalized Cdots is a valuable approach for the new generation of low-cost, green smart windows of energy efficient buildings. The figures of merit are: 1) simple, clean, fast, and nontoxic synthesis; 2) high conductivity and viscosity; 3) thermally induced nanoscopic memory effect that results in self-improving conductivity at consecutive heating/cooling cycles; 4) UV solar absorption which increases with temperature; and 5) thermotropy at 30–40 °C. The material was successfully used in two types of self-healing smart devices: a passive glass-based TTD with SPRE-boosted performance for zero energy buildings, and a device integrating independent sun-actuated TT and voltage-actuated EC options for energy efficient buildings. The active ECD encompasses bright hot and dark cold modes, and features colossal values of CE together with impressive optical memory.

Future work will focus on the performance of the devices as a function of time and temperature. They will be subject to artificial weathering tests in order to access the product durability. Tests will be performed under standard test conditions (AM1.5G solar simulator) and under real daylight conditions. The study will span a wide range of temperatures, including the low-temperature end below room temperature (down to −30 °C). The lifecycle assessment is of prime importance when practical applications of smart windows in sustainable buildings are envisaged. In the present case, such studies require extreme care given the complex nature of the nanofluid characterized by self-organization. Each heating and cooling cycle pushes the nanofluid to different metastable states, one of the consequences being the unique self-improving conductivity effect observed.

This work paves the way for the synthesis of other Cdots/IL nanofluids, and opens a window of exciting opportunities and tremendous challenges for the energy field, and for a wide variety of other equally exciting domains.

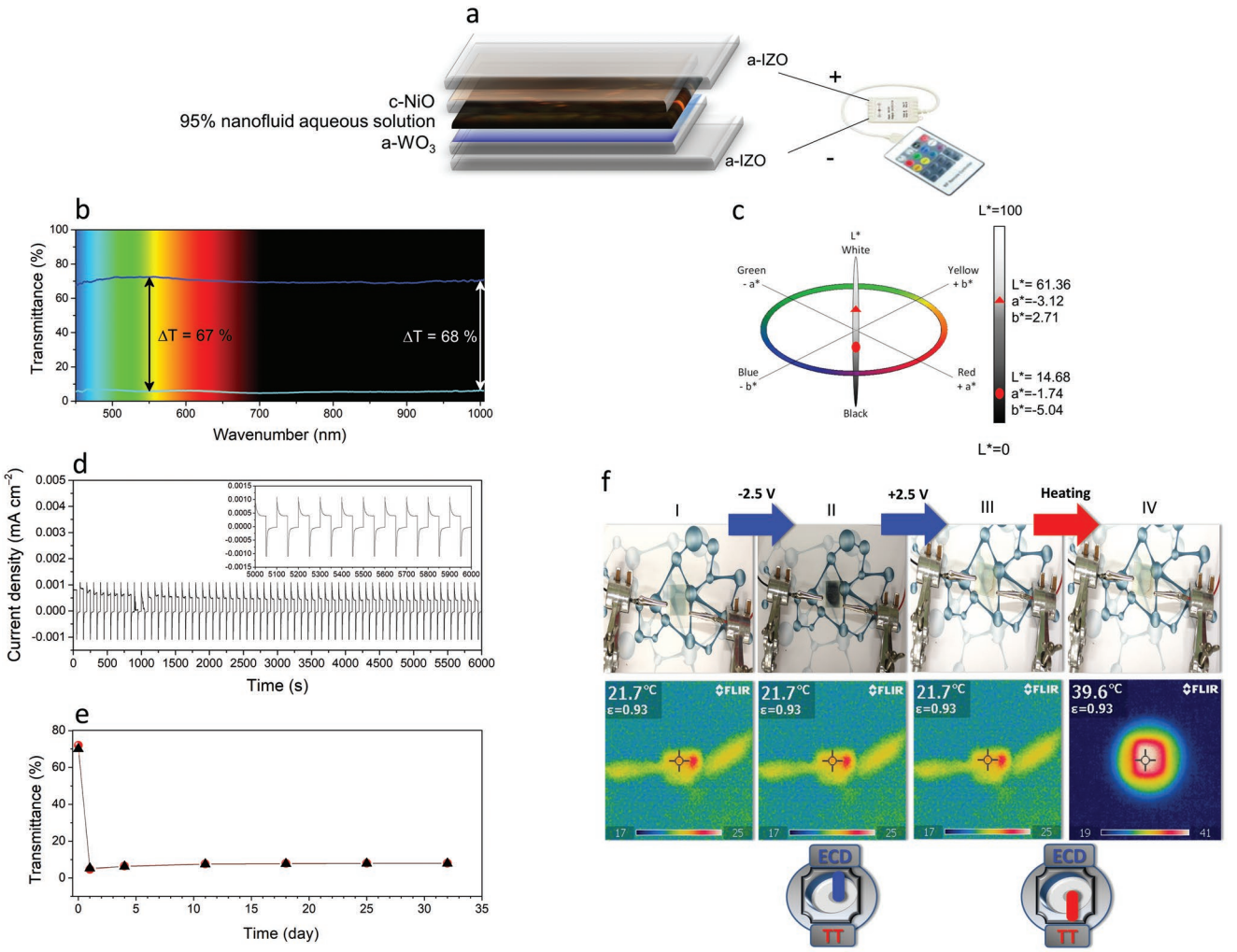

Figure 7. Performance of the ECD mode of the integrated glass/a-IZO/a-WO_3/95% w/w nanofluid aqueous solution/c-NiO/a-IZO/glass TTD/ECD system. a) Schematic representation. b) Transmission spectra in the bleached state/bright hot mode (blue line) and in the colored state/dark cold mode upon application of –2.5 V (cyanide line). c) CIE 1976 L*a*b* color diagram: as-deposited state (red triangle) and colored state at –2.5 V (red circle). d) Variation of the current density with voltage steps of ±2.5 V at every 50 s over 60 cycles. Inset of (d): zoom of last CA 10 cycles. Optical memory test upon application of –2.5 V. e) Transmittance values were registered at 550 nm (black symbols) and 1000 nm (red symbols). f) Independent operation of the integrated TT/EC device: visible photographs (top) illustrate the active operation of the integrated system operating as a pure ECD I–III) and as a pure TTD III,IV). ECD operation: coloring (–2.5 V) I,II) and bleaching (+2.5 V) II,III) states. TTD operation: heating from room temperature to 39.6 °C. Infrared photographs (bottom) I–III) demonstrate that the temperature of the ECD did not change upon voltage application. Visible photographs (top) III,IV) demonstrate that the color of the TTD did not change during heating.

4. Experimental Section

Materials: Anhydrous glucose (analytical grade, Fisher Scientific) and 1-butyl-3-methylimidazolium chloride (98%, Merck and Acros Organics) were used as received. High-purity Milli-Q water (resistivity 18 MΩ cm, Interlab Sistem Purist UV set) was used to prepare the aqueous solution.

Synthesis of In Situ Functionalized [Bmim]Cl/C Dots Nanofluid: The single-step synthesis of Cdots was performed in a round-bottom flask with constant magnetic stirring. The Cdots were prepared by the addition of [Bmim]Cl to anhydrous glucose in a 1:5 w/w ratio. The resulting mixture was heated to 100 °C for 1 h and left to cool at room temperature. After cooling, the resulting Cdots presented a viscous consistency and a brown coloration. They were transferred into a dialysis cellulose tubing membrane with a molecular weight cut-off of 500 Da and were dialyzed against ultrapure water for 40 h. The resulting solution was centrifuged for 10 min at 5000 rpm and the supernatant was extracted and centrifuged again. This procedure was repeated thrice, until no solid could be separated from the solution. The resulting solution was lyophilized until no water was found (roughly 3 days). The purified Cdots had a viscous nanofluidic consistency at room temperature. Upon lyophilization, the nanofluid could easily be redispersed in water, ethanol, and acetone whenever necessary.

Characterizations Procedures: High-resolution transmission electron microscopy images were recorded at the International Iberian Nanotechnology Laboratory (INL)-Portugal on a JEOL JEM 2100 (200 kV) with UC-A on holey 400 mesh Cu grids (Ted Pella ref. 01824). The samples were prepared by drop-casting a solution of the sample in absolute ethanol onto a grid, followed by drying at room temperature. The AFM measurements were performed in a Nano-Observer AFM microscope (CSInstruments AFM Microscopes, France) using a taping mode, and a super sharp Si HQ:NSC19/FORTA probe with a frequency resonance of 60 kHz and a spring constant of 0.3 N m^{-1}. Flattening and elimination of line noise tools and a low-pass filter were provided by the Gwyddion 2.52 software to improve the quality of the images.

The determination of the number of NPs in the measurements was performed using marked border detection with a Laplace edge tool of Gwyddion 2.52 software. SEM and energy dispersive X-ray spectroscopy (EDS) measurements were acquired in a TableTop SEM Model EM-30AXPlus (COXEM, Korea/Measurements performed by ScienTec, France) and a Bruker Quantax Flash 630, respectively, using an absolute ethanol dilute solution. TGA was performed using a TG209 F3 Tarsus thermogravimetric analyzer (Netzsch Instruments) under a nitrogen atmosphere with a heating rate of 10 °C min^{-1}. UV–vis spectra were recorded using a UV–vis spectrophotometer (U-4100). Dynamic viscosity measurements were carried out on a rheometer (Brookfield DV-II) with a cone-plate system (SSA spindle 21). Conductivity measurements were performed on WPA CM35 analog conductivity meter with a homemade probe with a constant value of 0.5468 cm^{-1}. Both the viscosity and the conductivity sample holder were kept in a thermostatic bath in a Julabo F25 between about 5 and 60 °C. The Zeta Potential was measured with a Zeta PALS potential analyzer (Brookhaven, USA) with parallel-plate platinum black electrodes spaced 5 mm apart and a 10 mm path length rectangular organic glass cell. All the samples were measured using a sinusoidal voltage of 80 V with a frequency of 3 Hz. For each sample, a total of ten values were automatically given by the instrument, which were then averaged to give the final value and the standard deviation.

TTD Assembly: Two TTDs were built. Prior to their assembly, static contact angle measurements (sessile drop method) of the aqueous solution with different concentrations of the nanofluid were performed using a clean glass plate and also a Ag-decorated glass plate as substrates. The results demonstrated that the 95% concentration of nanofluid was an optimal concentration to ensure the best adhesion of the nanofluid to the glass surface. In order to maintain the same conditions, this was also the concentration used for the integrated ECD described below. For the assembly of the first TTD, a volume of 100 µL of the slightly viscous 95% nanofluid aqueous solution was spread in between 2 cm × 4 cm glass plates and a 0.133 mm thick film with a brownish hue was formed (Figure 6a). In the case of the second TTD, silver (Ag) islands were first produced on a glass plate by the annealing process.[41,45] The 95% nanofluid aqueous solution was then sandwiched between the Ag-decorated glass plate and a clean glass plate (Figure 6b), ensuring the same thickness of the nanofluid film employed in the above TTD lacking Ag islands (0.133 mm). The plasmonic effect is mainly dependent on the size, shape, and interparticles distance. By assuring the same metal constitution and film thickness, the results may be interpreted as a function of the different intrinsic characteristics of the synthetized nanofluid.

ECD Assembly: The active layers of the ECD device (a-WO_3 and c-NiO) were deposited by sputtering and e-beam evaporation, respectively, on a-IZO glass previously deposited by sputtering. The amorphous a-WO3 was produced in an argon and oxygen atmosphere (oxygen partial pressure of 0.2 Pa) and a deposition pressure of 1.0 Pa, under an r.f. power of 200 W in a Pfeiffer Vacuum Classic 500 system using 3 diameter ceramic target from Plasmaterials, thus achieving a thickness of 300 nm. A polycrystalline c-NiO film with a 300 nm thickness was obtained from NiO commercial pellets random pieces 3–6 mm (99.99%, Super Conductive Materials) and deposited by e-beam evaporation in a homemade system, with an initial chamber pressure of 7×10^{-4} Pa and growth rate of 6 nm min^{-1}. The a-IZO thin films (resistivity of 7.97×10^{-4} Ω cm, mobility of 52.1 cm^2 V^{-1} s^{-1}, and carrier concentration of 1.50×10^{20} cm^{-3}) were deposited by sputtering, in a homemade system, from In_2O_3/ZnO 89.3/10.7 wt%, 99.99%, 3 in. dia × 6 mm thick (Super Conductive Materials). The sputtering process was carried out at a constant 0.13 Pa value (argon and oxygen) and room temperature. The substrate and target were apart by 10 cm and the r.f. power was 100 W. AFM images of the a-IZO, a-WO_3, and c-NiO layers were recorded in an AFM CSI Nano-Observer equipment (Scientec) in tapping mode using a super sharp Si HQ:NSC19/FORTA probe with a frequency resonance of 60 kHz and a spring constant of 0.3 N m^{-1}.

ECD Characterization: The ECD optical transmittance was measured in the 400–1020 nm range using a DH Mini, UV–vis–NIR Lightsource Ocean Optics and a halogen lamp. The CV and CA tests were carried out using a Gamry potentiostat/galvanostat ZRA 11107. In the setup used for measurements, the a-WO3/a-IZO substrate played the role of working electrode, the electrolyte acted as a reservoir of ions for insertion, and the c-NiO/a-IZO substrate acted as counter and reference electrodes. The cathodic and anodic charge densities were obtained through the CA curves integration during the coloring and bleaching processes, respectively. The Commission Internationale d'Éclairage (CIE) 1976 L*a*b* color space ECD coordinates were obtained with a Chroma Meter CR-300 Minolta (Osaka, Japan). The L*, a*, and b* parameters (L* is the lightness, a* represents the green–red component, and b* represents the blue–yellow component) were calculated from the average values obtained from three independent measurements in different places of the window.

ECD Video Method: A 3.25 cm^2 window was prepared as described above. In the video, it is possible to see the switching between the colored and bleached states upon application of −2.5 and 2.5 V, respectively. Additionally, the window was disassembled and assembled again in order to illustrate the device self-healing effect. The connections were consecutively reversed to access the bleached/colored state. At last, upon disassembly of the device, another coloring/bleaching cycle was performed proving that its electro-optical characteristics remained unaltered.

Supporting Information

Supporting Information is available from the Wiley Online Library or from the author.

Acknowledgements

This research was funded by the National Funds by Foundation for Science and Technology (FCT) and by the FEDER funds through POCI-COMPETE 2020-Operational Programme Competitiveness and Internationalization in Axis I: Strengthening research, technological development and innovation (UID/QUI/00616/2013, UID/QUI/50006/2019, UID/Multi/00709/2013, UID/QUI/00313/2019, UID/CTM/50025, POCI-01-0145-FEDER-007491, POCI-01-0145-FEDER-007688, UID/CTM/50025, POCI-01-0145-FEDER-016884, PTDC/CTM-NAN/0956/2014, SAICT/PAC/0032/2015, POCI-01-0145-FEDER-016422, and NORTE-01-0145-FEDER-030858). R.F.P.P. acknowledges FCT-MCTES for SFRH/BPD/87759/2012 grant. R. Rego and M. Fernandes (UTAD, Vila Real) and E. Pereira (FCUP, Porto) are acknowledged for their assistance.

Conflict of Interest

The authors declare no conflict of interest.

Keywords

carbon dots, integrated thermotropic–electrochromic devices, ionic liquids, self-regenerating, smart windows

Received: April 8, 2019
Revised: May 18, 2019
Published online:

[1] B. K. Sovacool, *Nature* **2014**, *511*, 529.
[2] UNESCO, Tech. Rep. 2017, https://unesdoc.unesco.org/ark:/48223/pf0000247785?posInSet=3&queryId=7367099e-2ad3-4a27-8c2b-5edf74ff812f (accessed: May 2019).
[3] F. Pacheco-Torgal, M. V. Diamanti, A. Nazari, C. S. Granqvist, *Nanotechnology in Eco-Efficient Construction*, Woodhead Publishing, New York, USA **2018**.

[4] Independent Statistics & Analysis, U.S. energy Information Administration, https://www.eia.gov/tools/faqs/faq.php?id=86&t=1 (accessed: May 2019).
[5] G. B. Smith, C. S. Granqvist, *Green Nanotechnology: Solutions for Sustainability and Energy in the Built Environment*, CRC Press, Boca Raton **2010**.
[6] A. Ghosh, B. Norton, *Renewable Energy* **2018**, *126*, 1003.
[7] K. Goossens, K. Lava, C. W. Bielawski, K. Binneman, *Chem. Rev.* **2016**, *116*, 4643.
[8] H. Ohno, *Electrochemical Aspects of Ionic Liquids*, John Wiley & Sons, New York, USA **2005**.
[9] D. R. MacFarlane, N. Tachikawa, M. Forsyth, J. M. Pringle, P. C. Howlett, G. D. Elliott, J. H. Davis, M. Watanabe, P. Simon, C. A. Angellg, *Energy Environ. Sci.* **2014**, *7*, 232.
[10] M. Watanabe, M. L. Thomas, S. Zhang, K. Ueno, T. Yasuda, K. Dokko, *Chem. Rev.* **2017**, *117*, 7190.
[11] D. R. MacFarlane, M. Forsyth, P. C. Howlett, M. Kar, S. Passerini, J. M. Pringle, H. Ohno, M. Watanabe, F. Yan, W. Zheng, S. Zhang, J. Zhang, *Nat. Rev. Mater.* **2016**, *1*, 15005.
[12] K. Fujita, R. Nakano, R. Nakaba, N. Nakamura, H. Ohno, *Chem. Commun.* **2019**, *55*, 3578.
[13] H. Hajfarajollah, B. Mokhtarani, A. Sharifi, M. Mirzaeia, A. Afaghia, *RSC Adv.* **2014**, *4*, 13153.
[14] A. Efimova, G. Hubrig, P. Schmidt, *Thermochim. Acta* **2013**, *573*, 162.
[15] O. Ryosuke, H. Satoshi, S. Satyen, K. Akiko, H. Hiro-o, *Chem. Lett.* **2013**, *32*, 948.
[16] J. D. Holbre, W. M. Reichert, M. Nieuwenhuyzen, S. Johnston, K. R. Seddonb, R. D. Rogers, *Chem. Commun.* **2003**, *0*, 1636.
[17] H. Satochi, R. Ozawa, H. Hamaguchi, *Chem. Lett.* **2003**, *32*, 498.
[18] S. Satyen Saha, H. Satoshi, K. Akiko, H. Hiro-o, *Chem. Lett.* **2003**, *32*, 740.
[19] R. Das, R. Bandyopadhyay, P. Pramanikc, *Mater. Today Chem.* **2018**, *8*, 96.
[20] H. M. R. Gonçalves, A. J. Duarte, J. C. G. E. Silva, *Biosens. Bioelectron.* **2010**, *26*, 1302.
[21] L. Efremushkin, S. K. Bhunia, R. Jelinek, A. Salomon, *J. Phys. Chem. Lett.* **2017**, *8*, 6080.
[22] Y. Zhang, H. Gonçalves, J. C. G. E. da Silva, C. D. Geddes, *Chem. Commun.* **2011**, *47*, 5313.
[23] S. Hill, M. C. Galan, *Beilstein J. Org. Chem.* **2017**, *13*, 675.
[24] J. Zhang, S. Yu, *Mater. Today* **2016**, *19*, 382.
[25] B. A. K. Naik, A. Vinod, *Exp. Therm. Fluid Sci.* **2018**, *90*, 132.
[26] P. Sharma, I.-H. Baek, T. Cho, S. Park, K. B. Leed, *Powder Technol.* **2011**, *208*, 7.
[27] M. Ahmadi, G. Willing, *Int. J. Heat Mass Transfer* **2018**, *118*, 40.
[28] B. P. V. Heiz, Z. Pan, L. Su, S. T. Le, L. Wondraczek, *Adv. Sustainable Syst.* **2018**, *2*, 1700140.
[29] B. P. V. Heiz, Z. Pan, G. Lautenschläger, C. Sirtl, M. Kraus, L. Wondraczek, *Adv. Sci.* **2017**, *4*, 1600362.
[30] L. Su, M. Fraaß, M. Kloas, L. Wondraczek, *Front. Mater.* **2019**, *6*, 102.
[31] Y. Chen, Q. Yang, P. Xu, L. Sun, D. Sun, K. Zhuo, *ACS Omega* **2017**, *2*, 5251.
[32] G. E. Croy, S.-T. Yang, F. Yang, Y. Liu, K. A. S. Fernando, C. E. Bunker, Y. Hu, P. G. Luo, Y.-P. Sun, *Coord. Chem. Rev.* **2016**, *320*, 66.
[33] J. Briscoe, A. Marinovic, M. Sevilla, S. Dunn, M. Titirici, *Angew. Chem., Int. Ed.* **2015**, *54*, 4463.
[34] H. Li, L. Chen, H. Wu, H. He, Y. Jin, *Langmuir* **2014**, *30*, 15016.
[35] C. Wang, C. Wang, P. Xu, A. L. Yujuan, C. K. Zhuo, *J. Mater. Sci.* **2016**, *51*, 861.
[36] A. Pal, G. Natu, K. Ahmada, A. Chattopadhyay, *J. Mater. Chem. A* **2018**, *6*, 4111.
[37] X. Sun, Q. Zhang, K. Yin, S. Zhou, H. Li, *Chem. Commun.* **2016**, *52*, 12024.
[38] T. Kato, M. Yoshio, T. Ichikawa, B. Soberats, H. Ohno, M. Funahashi, *Nat. Rev. Mater.* **2017**, *2*, 17001.
[39] S. Halelfadl, P. Estellé, B. Aladag, N. Doner, T. Maré, *Int. J. Therm. Sci.* **2013**, *71*, 111.
[40] L. D. Carlos, V. de Zea Bermudez, V. S. Amaral, S. C. Nunes, N. J. O. Silva, R. A. Sá Ferreira, J. Rocha, C. V. Santilli, D. Ostrovskii, *Adv. Mater.* **2007**, *19*, 341.
[41] P. W. Anderson, *Science* **1972**, *177*, 393.
[42] M. M. Waldrop, *Complexity: The Emerging Science at the Edge of Order and Chaos*, Touchstone, New York **1992**.
[43] I. Prigogine, *Order Out of Chaos*, Bantam Books, New York **1984**.
[44] P. E. Anderson, H. J. Jensen, L. P. Oliveira, P. Sibani, *Complexity* **2004**, *10*, 49.
[45] A. Agrawal, I. Kriegel, D. Milliron, *J. Phys. Chem. C* **2015**, *119*, 6227.
[46] W. C. Liao, Y.-M. Liao, C.-T. Su, P. Perumal, S.-Y. Lin, W.-J. Lin, C.-H. Chang, H.-I. Lin, G. Haider, C.-Y. Chang, S.-W. Chang, C.-Y. Tsai, T.-C. Lu, T.-Y. Lin, Y.-F. Chen, *ACS Appl. Nano Mater.* **2018**, *1*, 152.
[47] S. W. Oh, S.-H. Kim, T.-H. Yoon, *Adv. Sustainable Syst.* **2018**, *2*, 1800066.
[48] D. Cao, C. Xu, W. Lu, C. Qin, S. Cheng, *Sol. RRL* **2018**, *2*, 1700219.
[49] K. Aslan, Z. Leonenko, J. R. Lakowicz, C. D. Geddes, *J. Fluoresc.* **2005**, *15*, 643.
[50] N. C. Davy, M. Sezen-Edmonds, J. Gao, X. Lin, A. Liu, N. Yao, A. Kahn, Y.-L. Loo, *Nat. Energy* **2017**, *2*, 17104.
[51] M. A. Cardoso, R. F. P. Pereira, S. Pereira, H. Gonçalves, M. M. Silva, L. D. Carlos, S. C. Nunes, E. Fortunato, R. A. S. Ferreira, R. Rego, V. de Zea Bermudez, *Adv. Sustainable Syst.* **2019**, *3*, 1800115.
[52] S. C. Nunes, S. M. Saraiva, R. F. P. Pereira, S. Pereira, M. M. Silva, L. D. Carlos, E. Fortunato, R. A. S. Ferreira, R. Rego, V. de Zea Bermudez, *ACS Appl. Energy Mater.* **2019**, *2*, 1951.
[53] S. Pereira, A. Gonçalves, N. Correia, J. Pinto, L. Pereira, R. Martins, E. Fortunato, *Sol. Energy Mat. Sol. Cells* **2014**, *120*, 109.

